Mixed Quantum-Classical Reaction Path Dynamics of $C_2H_5F \rightarrow C_2H_4 + HF$

Christopher J. Stopera,[†] Landon L. Bladow, W. David Thweatt,[‡] and Michael Page*

Department of Chemistry and Molecular Biology, North Dakota State University, Fargo, North Dakota 58105

Received: July 9, 2008; Revised Manuscript Received: August 22, 2008

A mixed quantum-classical method for calculating product energy partitioning based on a reaction path Hamiltonian is presented and applied to HF elimination from fluoroethane. The goal is to describe the effect of the potential energy release on the product energies using a simple model of quantized transverse vibrational modes coupled to a classical reaction path via the path curvature. Calculations of the minimum energy path were done at the B3LYP/6-311++G(2d,2p) and MP2/6-311++G** levels of theory, followed by energy-partitioning dynamics calculations. The results for the final HF vibrational state distribution were found to be in good qualitative agreement with both experimental studies and quasiclassical trajectory simulations.

I. Introduction

The dynamics and kinetics of three- and four-centered elimination of HF and HCl from halogenated alkanes have been the subject of a considerable number of experimental[1−25] and computational[26−35] studies. Initially, chemically activated decomposition by radical recombination was performed to obtain dynamical data,[1−11] and shock tube pyrolysis was used to obtain kinetic data.[12,13] Later, product energy distributions were measured via infrared multiphoton dissociation (IRMPD) experiments.[14−18] More recently, chemical activation has once again been used to investigate product energy distributions and determine the effects of various substituents.[19−22,24,25] Some of these later experimental studies have also included computational modeling results.[23,25]

Nonstatistical vibrational energy distributions of the HF product for the unimolecular decomposition of fluoroethane and related molecules have been obtained by monitoring HF infrared emission following infrared multiphoton dissociation[17] and chemically activated decomposition.[19] The explanation, elaborated upon by Zamir and Levine,[36] was that the available energy may be divided into two portions: the barrier height of the reverse reaction and the energy in excess of this barrier height. On the basis of RRKM theory, the excess energy is distributed statistically among the transition state vibrational modes.[36] However, the reverse barrier energy is distributed on the basis of the forces arising from the potential energy surface.[33]

It has been deduced from experiment that most of the energy deposited in the HF stretching vibration comes from the potential energy release. In the chemical activation study by Arunan, Wategaonkar, and Setser on HF elimination from fluoroethane,[19] it was found that only 1.92 kcal/mol, out of 13.47 kcal/mol HF vibrational excitation, came from the excess energy, while the remainder (11.55 kcal/mol) arose from the potential energy release. Most of the excess energy remains in the hydrocarbon fragment. Experimental studies focusing on product energy partitioning often observe emission from the HF fragment. Hence, it is important to understand how the potential energy is released into the HF product. Various models based on experiment have attempted to explain the release of the potential energy, including Berry's bootstrap model[37] and its extension by Holmes and Setser.[9,11]

A pioneering theoretical study was performed by Kato and Morokuma on HF elimination from fluoroethane.[27] They calculated the structure of the transition state and the intrinsic reaction coordinate (IRC) to investigate the mechanistic details for this reaction. Product energy partitioning was also analyzed in terms of a simple dynamical model. The vibrational enhancement of the HF fragment was attributed to the reaction path curvature, in that the IRC changes from HF stretching to relative translation during the elimination. Thus, the curvature coupling elements between the reaction coordinate and transverse vibrational modes are important in determining energy transfer to or from vibrational motion.[38]

Trajectory calculations have also been used to investigate HX elimination reactions. Classical trajectories along analytic potential energy surfaces have been used to study HF elimination from 1,1,1-trifluoroethane[28] and 1,2-difluoroethane.[29] Classical trajectories can also be calculated directly using ab initio electronic energies, gradients, and Hessians instead of an analytic potential energy surface. These direct dynamics simulations were once performed at the HF/3-21G level of theory for the decomposition of vinyl fluoride,[39] but recently quasiclassical direct dynamics studies have been performed at MP2/6-31G* and MP2/6-311++G** for HF elimination from fluoroethane.[33−35] Direct dynamics simulations have also been performed for a variety of HX eliminations from fluoroalkenes.[40−43] Other theoretical work has involved characterizing transition states and computing rates for HX elimination reactions.[26,30−32]

As an alternative to trajectory calculations, a reaction path Hamiltonian (RPH) approach can be used,[44−48] as was essentially done by Kato and Morokuma.[27] The popular RPH of Miller, Handy, and Adams describes the dynamics of the reacting system as motion along the minimum energy path with harmonic walls, so only a relatively small number of quantum chemistry calculations of the potential energy surface are required.[44] Several methods of solving the reaction path Hamiltonian have been developed.[49] The system/bath approach generally divides the dynamics into a "system" and a "bath", for example, the reaction coordinate and the transverse vibrations, or vice versa. An attempt is then made to eliminate the bath degrees of freedom, leaving only the system, and the bath's effects on it, to deal with. Although the simplest means of doing

* Corresponding author. E-mail: mike.page@ndsu.edu.
[†] Current address: Department of Chemistry, University of Missouri, Columbia, MO 65211.
[‡] Current address: Philip Morris Research Center, Richmond, VA 23234.

10.1021/jp806071g CCC: $40.75
Published on Web 10/25/2008

this is to treat the bath classically and the system quantum mechanically (a mixed quantum-classical approach), a fully quantum mechanical approach is possible.[50−53] Quantum methods often involve a time-dependent self-consistent field (TDSCF) algorithm, which has also been extended to a multiconfigurational TDSCF approach to address the effect of the bath on the rate of tunneling.[52]

Kato and Morokuma used a system/bath approach in which they treated the vibrational modes quantum mechanically and the reaction path classically.[27] Using this approach, they calculated the distribution of energy among the product vibrational modes. However, they did not obtain state-resolved populations for the vibrational modes. Billing also used a quantum-classical system/bath approach treating rotation and reaction path motion classically and transverse vibrations quantum mechanically.[45] He was able to obtain vibrational state distributions for, for example, $H + Cl_2 \rightarrow HCl + Cl$ and $H_2 + OH \rightarrow H_2O + H$. Reviews of this classical path method for dynamics[54] and the use of the RPH for mechanistic insight[55] are available.

In the present study, we also use a system/bath approach in which the vibrations are treated quantum mechanically and the reaction path is treated classically.[56] We construct our wave function as a product over vibrational modes, where the wave function for each mode is expanded in a harmonic oscillator basis (representing the individual quantum states). In this way, we are able to resolve the dynamics to give state information, the result of which is that the final state populations are obtained and can be compared to experimental and computational data. Our goal is to present a simple and tractable model that scales favorably with system size and qualitatively describes energy disposal from the potential energy surface to product vibrational modes. We present the derivation of the equations of motion along the reaction path in section II. Section III illustrates the application of these equations with calculations of the dynamics of HF elimination from fluoroethane using density functional theory (B3LYP/6-311++G(2d,2p)) and second-order Møller−Plesset perturbation theory (MP2/6-311++G**) and comparisons of the results to previous experimental and theoretical studies. Section IV summarizes our general results.

II. Methodology

We start with the reaction path Hamiltonian of Miller, Handy, and Adams for zero total angular momentum,[44]

$$H = \sum_{k=1}^{F-1}\left(\frac{1}{2}P_k^2 + \frac{1}{2}\omega_k(s)^2 Q_k^2\right) + V_0(s) + \frac{1}{2}\frac{[p_s - \sum_{k,l=1}^{F-1} Q_k P_l B_{k,l}(s)]^2}{[1 + \sum_{k=1}^{F-1} Q_k B_{k,F}(s)]^2} \quad (1)$$

where s and p_s are the coordinate and momentum for motion along the reaction path, $\{Q_k,P_k\}$ are the $F - 1$ coordinates and momenta for vibrations orthogonal to the reaction path ($F = 3N - 6$, N = number of atoms), $\omega_k(s)$ is the frequency of the kth normal mode, $V_0(s)$ is the potential energy along the reaction path (including the vibrational zero-point energy), and $B_{k,l}(s)$ is a coupling term defined as

$$B_{k,l} = \left\langle \frac{\partial}{\partial s}\mathbf{L}_k | \mathbf{L}_l \right\rangle \quad (2)$$

where $\mathbf{L}_k$ is the kth eigenvector of the mass-weighted Hessian, for which rotations and the reaction path have been projected out. The special case where $l = F$ is the coupling of the kth mode to the reaction path. This is the coupling of the reaction path to a vibrational mode due to curvature of the reaction path. The curvature coupling element (or mode-path coupling) for mode k can be found as

$$B_{k,F} = -\left\langle \frac{\partial}{\partial s}\boldsymbol{\nu} | \mathbf{L}_k \right\rangle \quad (3)$$

where ν, the reaction path tangent, is the negative of the normalized gradient. The total scalar curvature is thus defined as

$$\kappa = \left(\sum_{k=1}^{F-1} B_{k,F}(s)^2\right)^{1/2} \quad (4)$$

We consider the case where direct coupling between modes is negligible ($B_{k,l\neq F} = 0$), and the vibrational modes couple to the reaction path through the reaction path curvature. Expanding the denominator of eq 1 as a Taylor series and truncating after the linear term leads to

$$H = \sum_{k=1}^{F-1}\left(\frac{1}{2}P_k^2 + \frac{1}{2}\omega_k(s)^2 Q_k^2\right) + V_0(s) + \frac{1}{2}p_s^2 - p_s^2\sum_{k=1}^{F-1} Q_k B_{k,F}(s) \quad (5)$$

Following Billing,[45] we treat the vibrations quantum mechanically while treating the reaction path classically. The quantum Hamiltonian is chosen as

$$\hat{H}_Q(\{\hat{Q}_k, \hat{P}_k\}) = \sum_{k=1}^{F-1}\left(\frac{1}{2}\hat{P}_k^2 + \frac{1}{2}\omega_k(s)^2\hat{Q}_k^2\right) - p_s^2\sum_{k=1}^{F-1}\hat{Q}_k B_{k,F}(s) \quad (6)$$

$$\hat{H}_Q(\{\hat{Q}_k, \hat{P}_k\}) = \sum_{k=1}^{F-1}\hat{h}_k - p_s^2\sum_{k=1}^{F-1}\hat{Q}_k B_{k,F}(s) = \hat{H}^0 + \hat{H'} \quad (7)$$

We choose our wave function to be a product of one-dimensional functions, one for each mode (Θ_k), which we choose to be sums over simple harmonic oscillator states (SHOS, $\varphi_{k,i}$):

$$\Psi(\{Q_k\}, t, s) = \prod_{k=1}^{F-1}\Theta_k(Q_k, t, s) = \prod_{k=1}^{F-1}\sum_i c_{k,i}(t, s)\varphi_{k,i}(Q_k) \quad (8)$$

$$\hat{h}_k\varphi_{k,i}(Q_k) = \left(\frac{1}{2}\hat{P}_k^2 + \frac{1}{2}\omega_k(s)^2\hat{Q}_k^2\right)\varphi_{k,i}(Q_k) = \varepsilon_{k,i}(s)\varphi_{k,i}(Q_k) \quad (9)$$

where i indexes the SHOS and $\varepsilon_{k,i}$ is the energy of basis state i of mode k. The SHOS are treated as basis functions, so the upper limit is chosen at the time of computation. Because the quantum Hamiltonian is a sum over modes and the wave function is a product over modes, we can address each mode individually.

The time-dependent Schrödinger equation for normal mode Θ_k is

$$i\hbar\frac{\partial}{\partial t}\Theta_k(Q_k, t, s) = \hat{H}_Q\Theta_k(Q_k, t, s) \quad (10)$$

Substituting the expansion of $\Theta_k(Q_k, t, s)$ into eq 10, left multiplying by $\varphi_{k,j}(Q_k)^*$, and integrating over Q_k (utilizing Hermite polynomial recursion relations) yields

$$i\hbar\dot{c}_{k,j}(t,s) = c_{k,j}(t,s)\varepsilon_{k,j}(s) - p_s^2 B_{k,F}(s)\sum_i c_{k,i}(t,s)V_{j,i}^k(s) \tag{11}$$

where

$$V_{j,i}^k = \left(\frac{i}{2a_k}\right)^{\frac{1}{2}}\delta_{j,i-1} + \left(\frac{i+1}{2a_k}\right)^{\frac{1}{2}}\delta_{j,i+1} \tag{12}$$

and

$$a_k = \frac{\omega_k(s)}{\hbar} \tag{13}$$

Substituting $c_{k,j}(t) = \alpha_{k,j}(t) + i\beta_{k,j}(t)$ into eq 11 and separating real and imaginary terms leads to

$$\hbar\dot{\alpha}_{k,j}(t,s) = \beta_{k,j}(t,s)\varepsilon_{k,j}(s) - p_s^2 B_{k,F}(s)\sum_i \beta_{k,i}(t,s)V_{j,i}^k(s) \tag{14}$$

and

$$-\hbar\dot{\beta}_{k,j}(t,s) = \alpha_{k,j}(t,s)\varepsilon_{k,j}(s) - p_s^2 B_{k,F}(s)\sum_i \alpha_{k,i}(t,s)V_{j,i}^k(s) \tag{15}$$

Equations 14 and 15 can be solved numerically using the value of p_s, the momentum along the reaction path, taken at each time step from the classical treatment of the reaction path motion.

To obtain the classical equations for the reaction path, we apply the mean-field approximation. The classical Hamiltonian is

$$H_{Cl} = \langle\Psi|H|\Psi\rangle = \langle\Psi|\hat{H}_Q|\Psi\rangle + V_0(s) + \frac{1}{2}p_s^2 \tag{16}$$

We treat $\hat{H}'$ in eq 7 as a time-dependent perturbation, so

$$\langle\Psi|\hat{H}_Q|\Psi\rangle = \sum_{k=1}^{F-1}\sum_j [\alpha_{k,j}(t,s)^2 + \beta_{k,j}(t,s)^2]\varepsilon_{k,j}(s) \tag{17}$$

From eq 17, we see that $\alpha_{k,j}(t)^2 + \beta_{k,j}(t)^2$ is the population probability of state j of mode k, and $\varepsilon_{k,j}$ is the energy of state j of mode k. Furthermore, eq 17 gives the total vibrational energy. So

$$H_{Cl} = E_{vib}(s) + V_0(s) + \frac{1}{2}p_s^2 \tag{18}$$

and from Hamilton's equations of motion,

$$\dot{s} = \frac{\partial H_{Cl}}{\partial p_s} = p_s \tag{19}$$

and

$$\dot{p}_s = -\frac{\partial H_{Cl}}{\partial s} = -\frac{d}{ds}E_{vib}(s) - \frac{d}{ds}V_0(s) \tag{20}$$

Substituting eq 17 into eq 20 and using the expression for the energy of SHOS yields

$$\dot{p}_s = -\left\{\sum_{k=1}^{F-1}\sum_j 2\left[\alpha_{k,j}(t,s)\frac{\dot{\alpha}_{k,j}(t,s)}{\dot{s}} + \beta_{k,j}(t,s)\frac{\dot{\beta}_{k,j}(t,s)}{\dot{s}}\right]\varepsilon_{k,j}(s) + [\alpha_{k,j}(t,s)^2 + \beta_{k,j}(t,s)^2]\left(j+\frac{1}{2}\right)h\frac{d}{ds}\nu_k(s)\right\} - \frac{d}{ds}V_0(s) \tag{21}$$

where $\nu_k(s) = \omega_k(s)/2\pi$. We now have two sets of coupled differential equations, eqs 14 and 15 and eqs 19 and 21. These equations are solved after the minimum energy path has been determined.

The computational details are as follows. First, a transition state is located for the reaction of interest. Once this geometry has been verified as the desired transition state, the minimum energy path (MEP, the path of steepest descent from transition state to products in mass-weighted Cartesian coordinates) is determined for the reaction. At each point along the MEP, the projected force constant matrix is calculated to determine the vibrational frequency (ν_k) as well as the curvature coupling element ($B_{k,F}$) for each mode. $V_0(s)$, $B_{k,F}(s)$, and $\nu_k(s)$ are then fit to analytic functions: linear combinations of Gaussian functions for $B_{k,F}(s)$ and $V_0(s)$ and a single Eckart function for $\nu_k(s)$. With these analytic functions, the coupled differential equations can be solved numerically; our implementation uses fourth-order Runge−Kutta integration. An excess kinetic energy of interest is chosen, usually a minimal 0.01 kcal/mol, along with corresponding initial conditions for a step size in time and the number of basis states that will give the desired accuracy. Convergence of results is assured by requiring conservation of energy to six significant figures and using at least 10 times as many basis states as there are populated states in the products.

III. Application to $C_2H_5F \rightarrow C_2H_4 + HF$

A. Features of the Minimum Energy Path. The method described above was used to investigate HF elimination from C_2H_5F. We augmented NWChem[57] to perform corrected local quadratic approximation (CLQA)[58] MEP calculations and used the program to determine the MEP. For determining stationary points, we used the default mode-following algorithm in NWChem for the transition state (TS) and the default quasi-Newton algorithm for the reactant and products. These calculations were done at the B3LYP/6-311++G(2d,2p) and MP2/6-311++G** levels of theory. The MP2 calculations were performed for comparison to quasiclassical direct dynamics trajectory simulations[34] using the same level of theory and basis set. No orbitals were frozen in the MP2 calculations, which were performed with the "tight" directive in NWChem for increased MP2 gradient and energy precision. The integration grid accuracy was set to the "fine" option in NWChem for the B3LYP calculations.

Geometrical parameters for the optimized reactant, transition state, and products at each level of theory are listed in Table 1. Models of the reactant and transition state are shown for reference in Figure 1. This reaction has a four-centered TS where, in the B3LYP case, the C−F and C−H bond lengths are stretched by 40% and 20%, respectively, from their values in the fluoroethane reactant. The C−C bond length in the TS is about 1.40 Å, which indicates roughly a 60% conversion from the single bond length in C_2H_5F to the double bond length in C_2H_4. A subsequent frequency calculation showed that the vector corresponding to the single negative eigenvalue points toward HF elimination (Figure 2a). For the MP2 TS, the parameters

TABLE 1: Geometric Parameters of the Optimized Reactant, Transition State, and Separated Products for $C_2H_5F \rightarrow C_2H_4 + HF$[a]

	level of theory					
	B3LYP/6-311++G(2d,2p)			MP2/6-311++G**		
parameter	reactant	TS	products	reactant	TS	products
R(H1−F)		1.332	0.922		1.290	0.917
R(C1−C2)	1.510	1.397	1.325	1.510	1.403	1.337
R(C2−F)	1.404	1.966		1.397	1.883	
R(C1−H1)	1.089	1.305		1.091	1.320	
R(C1−H2)	1.089	1.081	1.082	1.091	1.083	1.085
R(C1−H3)	1.091	1.081	1.082	1.094	1.083	1.085
R(C2−H4)	1.090	1.079	1.082	1.093	1.083	1.085
R(C2−H5)	1.090	1.079	1.082	1.093	1.083	1.085
∠H1−C1−C2	110.8	75.4		110.5	73.3	
∠F−C2−C1	109.9	91.8		109.7	93.3	
∠H2−C1−C2	110.8	118.9	121.7	110.5	118.6	121.4
∠H3−C1−C2	109.8	118.9	121.7	109.7	118.6	121.4
∠H4−C2−C1	112.0	121.6	121.7	111.7	121.1	121.4
∠H5−C2−C1	112.0	121.6	121.7	111.7	121.1	121.4
∠H1−C1−C2−F[b]	−60.4	0.0		−60.4	0.0	
∠H3−C1−C2−H1	−119.6	−103.3		−119.8	−102.9	
∠H3−C1−C2−H2	119.6	153.4	180.0	119.8	154.1	180.0
∠H3−C1−C2−H4	−61.4	−8.8	0.0	−61.6	−5.8	0.0
∠H3−C1−C2−H5	61.4	162.2	180.0	61.1	159.9	180.0

[a] Bond lengths are in angstroms, and bond angles are in degrees. The atom labels correspond to those in Figure 1. [b] Four-centered angles are dihedral angles.

agree to within 0.001 Å and 0.1° of the values calculated by Sun and Hase using the same level of theory and basis set[33] and are in fair agreement with higher level calculations.[34] The reactant and product geometries at both levels of theory agree well with both experimental[59] and computational[33] data.

From the TS, we performed a CLQA MEP calculation for $[C_2H_5F]^{\ddagger} \rightarrow C_2H_4 + HF$ using analytic Hessians at each step with B3LYP/6-311++G(2d,2p). For MP2/6-311++G**, Hessians were calculated by finite-difference of the analytic gradients. For a given step size along the reaction path, Δs, the CLQA more closely follows the actual MEP than Euler-based methods.[58] More accurate following of the reaction path leads to more accurate $\nu_k(s)$ and $B_{k,F}(s)$ values, which are important in reaction path dynamics. The MEP was calculated using a step size of 0.05 amu$^{1/2}$ bohr for 50 steps beyond the saddle point. Vectors for the direction of the reaction path (the reaction path tangent) at several values of s are shown in Figure 2 for the B3LYP calculation; the MP2 geometries and vectors are similar. Except at the saddle point, these images indicate the relative forces on the atoms as the system traverses the MEP; Figure 2b−e shows normalized negative reaction path gradients, while Figure 2a is the eigenvector corresponding to the imaginary frequency at the saddle point.

The B3LYP MEP calculation was run until the potential energy had dropped by 76%, which occurs at $s = 2.50$ amu$^{1/2}$ bohr. At $s = 1.50$ amu$^{1/2}$ bohr (see Figure 2e), the reaction path is relative translation of HF and C_2H_4. It remains as relative translation until $s = 1.90$ amu$^{1/2}$ bohr where it starts becoming HF rotation and C_2H_4 translation. This rotation seems to indicate the formation of a long-range van der Waals complex, which might be expected in the product region of the MEP. Even our energy-partitioning calculations with negligible excess energy above the transition state yield enough kinetic energy to break apart these long-range forces, so its formation is not pertinent to the reaction of interest. The scalar curvature has also diminished significantly by this point (see Figure 6). Furthermore, the geometries of the fragments at $s = 2.50$ amu$^{1/2}$ bohr deviate only slightly from the B3LYP/6-311++G(2d,2p) computed equilibrium geometries (Table 1) of HF and C_2H_4. The H−F bond length is 1.2% longer than its equilibrium value, the C−C bond length is 0.5% longer than its equilibrium value, and the C−H bonds are all within 0.1% of the equilibrium value. Also, the olefin fragment is within 3° of planarity. Thus, for our purposes, by $s = 2.50$ amu$^{1/2}$ bohr, the reaction of interest has finished.

Overall, the MP2 and B3LYP reaction paths display similar features. For the MP2 reaction path, the reaction of interest was also deemed complete at $s = 2.50$ amu$^{1/2}$ bohr, due to the same reasons given for the B3LYP path. At $s = 2.50$ amu$^{1/2}$ bohr, the potential energy has fallen by 77%, the H−F bond is 0.8% longer than its MP2/6-311++G** computed equilibrium value, the C−C bond is 0.4% longer than its equilibrium length, and the C−H bonds are all within 0.2% of the equilibrium value. The olefin fragment is within 5° of planarity.

Because there are $3N - 7$ bound degrees of freedom (N = number of atoms) for a nonlinear TS, there are 17 vibrational modes for the TS; however, there are only 13 vibrational modes for the products. Therefore, four of the TS vibrations must become rotational motions of the products. Observation of the normal mode eigenvectors near the end of the reaction path shows which modes become the necessary rotations. To account for these modes becoming rotations, their vibrational frequencies must become zero, and because the coupling elements $B_{k,F}(s)$ are defined specifically for vibrations (eq 3), they too must become zero. Although the frequencies of these modes generally decrease along the reaction path, they are usually not zero by the end of the reaction of interest due to the nature of MEP-following calculations, so it is often necessary to manually cause the curves to exponentially approach zero. This is illustrated in Figure 3 for the B3LYP vibrations.

The fundamental frequencies of the three normal modes that couple most strongly to the path at both levels of theory are shown in Figure 4, and their corresponding coupling elements ($B_{k,F}$) are displayed in Figure 5. As one might expect, these modes are strongly related to the overall reaction: one becomes the HF stretching motion, while the other two involve the

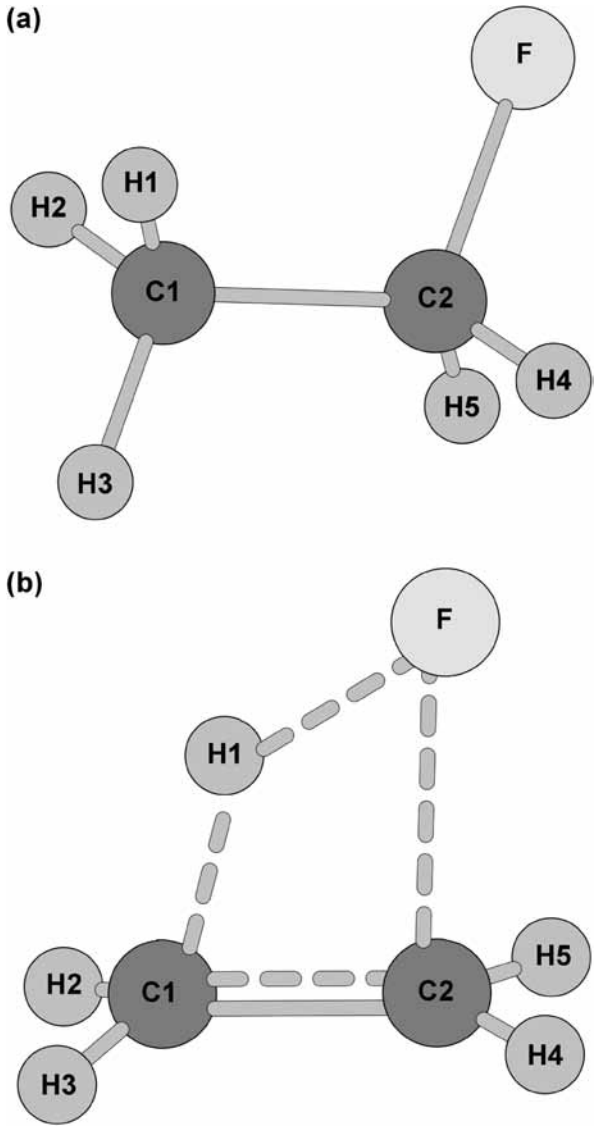

Figure 1. Geometry of the (a) staggered reactant and (b) transition state for the HF elimination from fluoroethane, determined at the B3LYP/6-311++G(2d,2p) level of theory.

asymmetric and symmetric out-of-plane CH_2 wagging motions of the olefin fragment. One would expect preferential excitation of these three modes when calculating the energy-transfer dynamics.

By looking at the total scalar curvature in Figure 6 and the vectors for the path tangents in Figure 2, we can divide the reaction into three primary parts and correlate these regions with the curvature coupling elements of the individual modes. This discussion focuses on the B3LYP calculations, but the three general regions are also observed with the MP2 calculations. The first part, from the TS ($s = 0.00$ amu$^{1/2}$ bohr) to $s = 0.50$ amu$^{1/2}$ bohr, consists of the formation of the HF bond and a stretching of the corresponding C−H and C−F bonds. There is little coupling in this region. The second part of the reaction, from $s = 0.50$ amu$^{1/2}$ bohr to $s = 1.50$ amu$^{1/2}$ bohr, is a transitional part. In this region, the motions of the H and F atoms are changing from HF bond formation to translation away from the C_2H_4 fragment. It is in this region that there is a substantial amount of curvature. We see from Figure 5 that this curvature is due primarily to the coupling to the reaction path of the mode that becomes the HF product's stretching motion. This mode makes up 97% of the total scalar curvature. It can be seen in

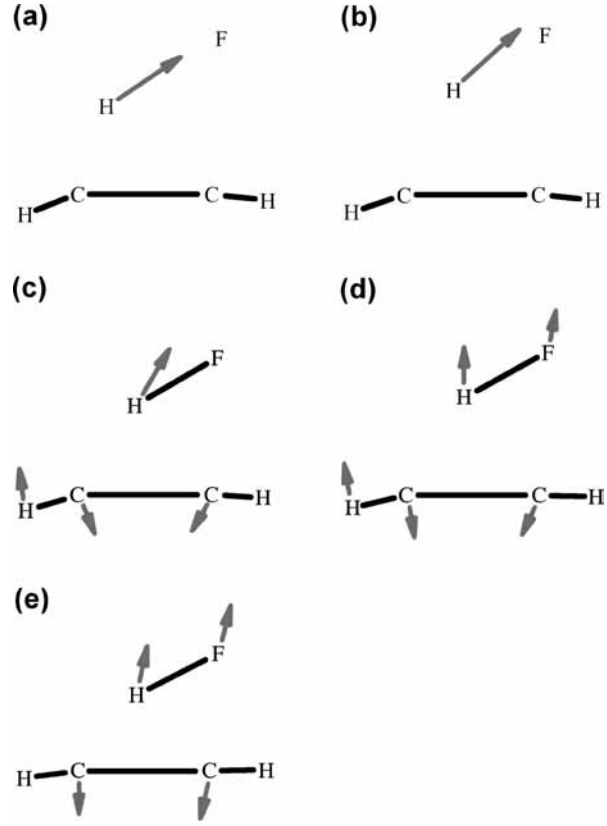

Figure 2. Direction of the B3LYP/6-311++G(2d,2p) reaction path at (a) $s = 0.00$ amu$^{1/2}$ bohr (transition state), (b) $s = 0.50$ amu$^{1/2}$ bohr, (c) $s = 0.75$ amu$^{1/2}$ bohr, (d) $s = 1.00$ amu$^{1/2}$ bohr, and (e) $s = 1.50$ amu$^{1/2}$ bohr. Note that these are 2D representations showing the plane of the four-centered TS, so two hydrogen atoms are not shown.

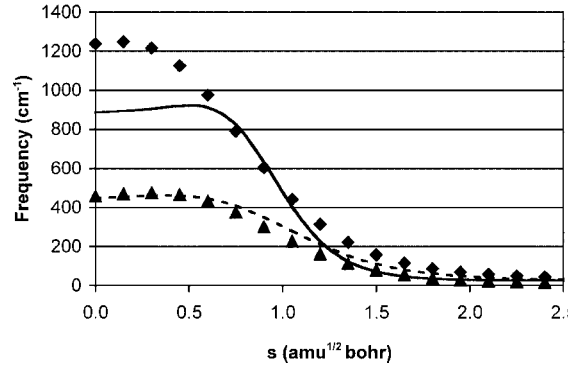

Figure 3. B3LYP/6-311++G(2d,2p) fundamental frequencies as a function of arc length along the reaction path for TS normal modes that become product rotational motions. Because these modes correspond to rotations in the products, their frequencies are made to exponentially approach 0 cm^{-1}.

Figure 4 that the frequency of this mode changes a great deal in this region as it becomes that of an isolated HF molecule.

It is important to note that it is not the relation between the vibration vector and the gradient vector that determines coupling, but rather the relation between the vibration vector and how the gradient vector is changing. When we look at the vector that describes the change in the gradient vector in this region, we find that it has a strong HF stretch component; we say that the path curves into the HF stretching mode as the reaction coordinate is traversed. This is why the HF stretching mode is able to couple so strongly to the reaction path in this region. This is in agreement with the early work of Kato and Morokuma.[27] The third part of the path is from $s = 1.50$ amu$^{1/2}$

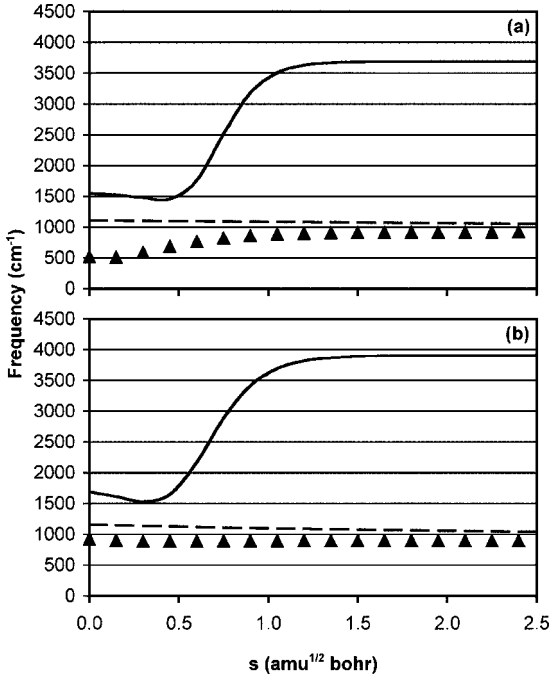

Figure 4. (a) B3LYP/6-311++G(2d,2p) and (b) MP2/6-311++G** fundamental frequencies as a function of arc length along the reaction path for the modes that couple most strongly to the path: asymmetric CH_2 wag (▲), symmetric CH_2 wag (dashed line), and HF stretch (solid line).

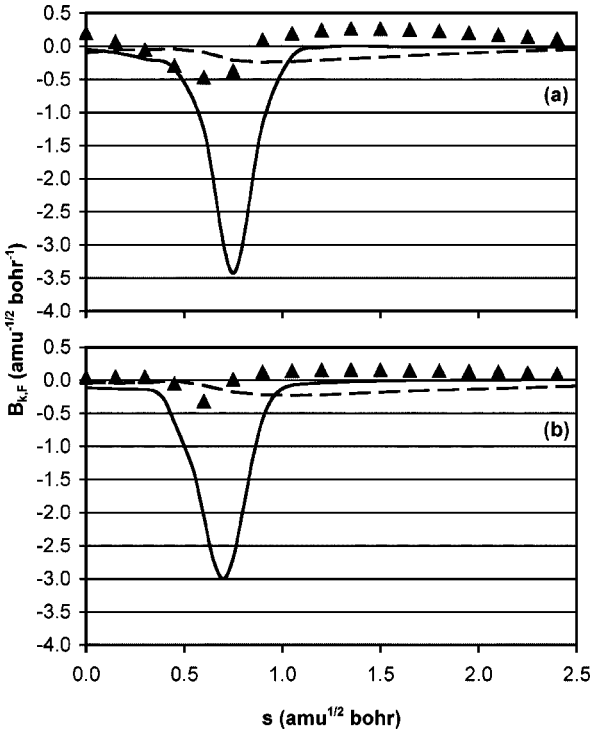

Figure 5. Curvature coupling as a function of arc length along the (a) B3LYP/6-311++G(2d,2p) and (b) MP2/6-311++G** reaction paths for the modes that couple most strongly to the path: asymmetric CH_2 wag (▲), symmetric CH_2 wag (dashed line), and HF stretch (solid line).

bohr to $s = 2.50$ amu$^{1/2}$ bohr. In this region, the HF fragment is moving away from the C_2H_4 fragment, and the C_2H_4 fragment is adjusting its bond lengths and angles. As in the first region, very little coupling occurs in this region. We expect that most distribution of energy among the vibrations is completed in the second region of the path and that, throughout the third region, energy is partitioned primarily into the kinetic energy along the path.

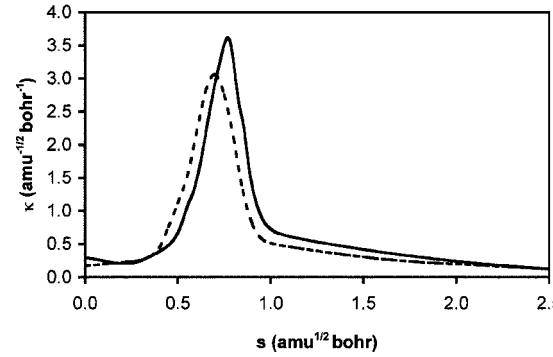

Figure 6. Total scalar curvature as a function of arc length along the B3LYP/6-311++G(2d,2p) reaction path (solid line) and the MP2/6-311++G** reaction path (dashed line).

TABLE 2: Thermochemical Parameters for $C_2H_5F \rightarrow C_2H_4 + HF$

	energy (kcal/mol)[a]		
parameter[b]	B3LYP/ 6-311++G(2d,2p)	MP2/ 6−311++G**	experiment[c]
$E_r°$	43.21	50.93	49.0 ± 2.0
$E_f°$	54.24	59.98	58.0 ± 1.0
ΔH_{0K}	11.03	9.05	9.0 ± 1.0
E_B	23.07	20.03	

[a] All values include zero-point energy corrections. [b] $E_r°$ is the barrier height for the reverse reaction, $E_f°$ is the barrier height for the forward reaction, ΔH_{0K} is the enthalpy change for the forward reaction at 0 K, and E_B is the energy lost by the time the scalar curvature drops below 0.50 amu$^{-1/2}$ bohr^{-1}. [c] From ref 6 and references therein.

A summary of the reaction energetics using both levels of theory is given in Table 2, along with the experimental values. As has been noted for other reactions,[60] the B3LYP exchange-correlation functional has underestimated the forward and reverse barrier heights for this reaction. The MP2 barrier heights and heat of reaction agree better with experimental values, and higher level theoretical values,[34] than do the B3LYP results. As compared to B3LYP, the MP2 reaction path has lost less of its potential energy by the end of major curvature (our E_B parameter); hence, one would predict less energy transfer to vibration in the MP2 case.

B. Energy-Partitioning Dynamics. ***1. B3LYP/6-311++G(2d,2p) General Analysis.*** After fitting $V_0(s)$, $B_{k,F}(s)$, and $\nu_k(s)$ to analytic functions, we are able to solve the set of coupled equations (eqs 14, 15, 19, and 21) numerically. The dynamics calculation is meant to investigate how the curvature of the path partitions the potential energy corresponding to the reverse barrier height (the "localized" or "fixed" energy).[17] To this end, we perform a calculation with essentially zero excess energy above the TS barrier. However, in practice, we need to nudge the system off the saddle point, so we use a negligible amount of excess energy, 0.01 kcal/mol, all in reaction coordinate translation. For this condition, it is sufficient to use a time step size of 0.01 bohr periods and 100 basis states.

By comparing the results of the overall B3LYP/6-311++G(2d,2p) reaction path dynamics shown in Figure 7 with the total scalar curvature in Figure 6, we see how the reaction path curvature affects the kinetic and vibrational energies. The path curvature acts as a pipe between the vibrational energy

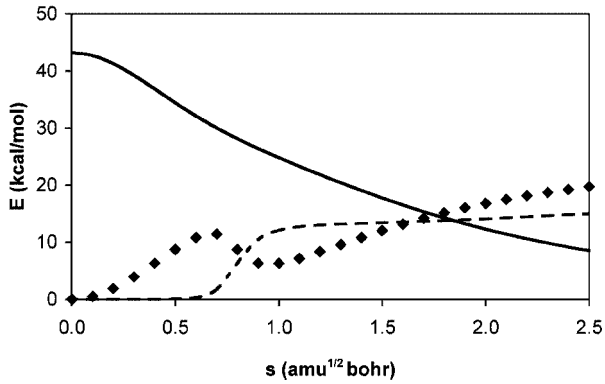

Figure 7. Overall energy-partitioning dynamics of HF elimination from fluoroethane for negligible excess energy (0.01 kcal/mol) calculated at the B3LYP/6-311++G(2d,2p) level of theory. The potential energy (plus zero-point energy) is shown as the solid line, the reaction path kinetic energy as ◆, and the vibrational energy (above the zero-point) as the dashed line.

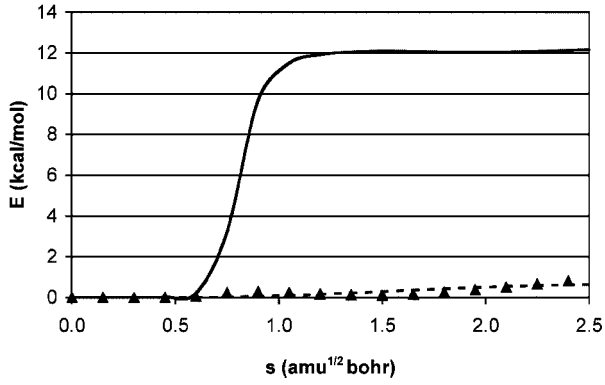

Figure 8. Vibrational mode energies above the zero-point as a function of arc length along the B3LYP/6-311++G(2d,2p) reaction path for the asymmetric CH_2 wag (▲), symmetric CH_2 wag (dashed line), and HF stretch (solid line) for the calculation with negligible excess energy (0.01 kcal/mol).

and the kinetic energy. As the curvature increases, the kinetic energy is more rapidly diverted into the vibrational degrees of freedom. This results in a rapid decrease in kinetic energy with a corresponding rapid increase in total vibrational energy. Once the reaction has passed this region of curvature, the vibrational modes experience little in the way of excitation, as shown in Figure 8, which shows the excitation of each normal mode. This is especially evident for the HF stretch in Figure 8, where it has rapid energy gain between $s = 0.50$ amu$^{1/2}$ bohr and $s = 1.50$ amu$^{1/2}$ bohr, but then levels off after $s = 1.50$ amu$^{1/2}$ bohr.

We also see from Figure 8 that, just as was expected on the basis of curvature, most of the vibrational energy is put into the HF stretch; this mode gains 12.2 kcal/mol, which is 84% of the total vibrational energy and 28% of the exit channel potential energy. This is in fair agreement with IRMPD and chemical activation studies, which indicated that 24% of the potential energy release ended up in the HF stretch.[17,19] The dynamics calculation further shows how the potential energy is partitioned into the states of each mode; that is, the population probability for each state of each mode is also acquired. The population probabilities for the HF stretch from our mixed quantum-classical calculations are compared to the population distribution obtained by IRMPD[17] in Figure 9 and show excellent agreement. Comparisons to the chemical activation experiment[19] and our MP2/6-311++G** results (see below) are also included in the figure. The B3LYP and MP2 results are in good agreement and show the same general trend as the chemical activation

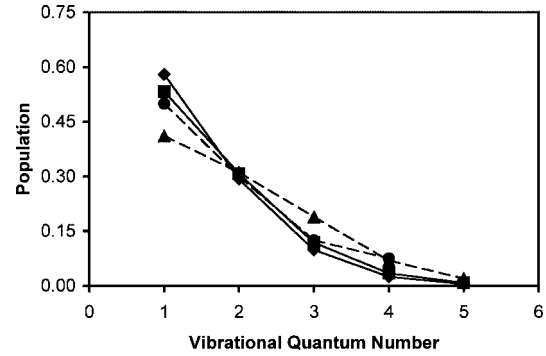

Figure 9. Comparison of HF stretch populations from theoretical (solid line) and experimental (dashed line) studies. Our B3LYP/6-311++G(2d,2p) quantum-classical results are shown as ■, our MP2/6-311++G** quantum-classical results as ◆, the IRMPD results (ref 17) as ●, and the chemical activation results (ref 19) as ▲. In all cases, the results are normalized to the sum of the populations of the first five excited vibrational states. The theoretical results are all for the negligible excess energy case.

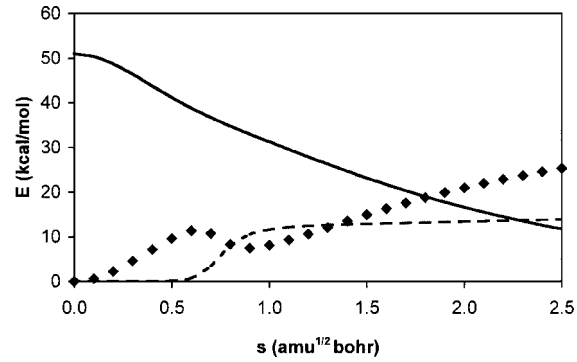

Figure 10. Overall energy-partitioning dynamics of HF elimination from fluoroethane for negligible excess energy (0.01 kcal/mol) calculated at the MP2/6-311++G** level of theory. The potential energy (plus zero-point energy) is shown as the solid line, the reaction path kinetic energy as ◆, and the vibrational energy (above the zero-point) as the dashed line.

population distributions, which arise from a greater amount of excess energy above the TS.[19]

2. MP2/6-311++G** Analysis and Comparisons. The primary purpose of our MP2 calculations was to allow direct comparison to the direct dynamics classical trajectory results of Dong et al.[34] Two energy-partitioning dynamics calculations were performed on the MP2/6-311++G** reaction path: one with negligible excess energy (0.01 kcal/mol) and one, following ref 34, with 3.45 kcal/mol above the TS zero-point energy. The excess energy in each case was added solely to reaction coordinate translation. The calculations were each performed with 200 basis states and a time step size of 0.01 bohr periods.

The overall energy-partitioning dynamics for the minimal excess energy case (0.01 kcal/mol) are displayed in Figure 10. This calculation was performed to see the effect of the potential energy release alone on the vibrational state populations and energy-transfer dynamics. It can be seen that, around the maximum curvature ($s = 0.70$ amu$^{1/2}$ bohr, Figure 6), kinetic energy is being transferred to vibrational energy and causing vibrational mode excitation. The energy gains of the three aforementioned modes that couple most strongly to the path are shown in Figure 11. The HF stretching mode obtains 11.3 kcal/mol, which corresponds to 22% of the potential energy release. The out-of-plane asymmetric CH_2 wag gains 0.6 kcal/mol, while the out-of-plane symmetric CH_2 wag obtains 1.0 kcal/mol; the other modes each obtain less than 0.5 kcal/mol.

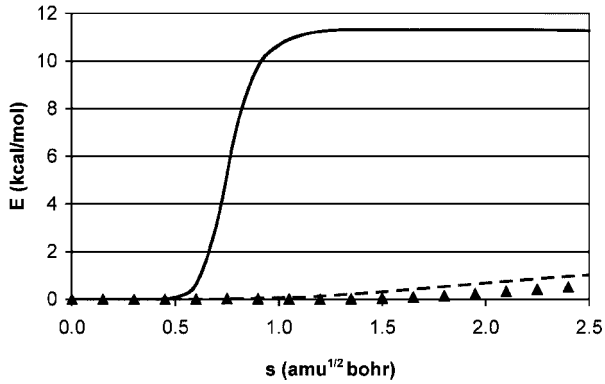

Figure 11. Vibrational mode energies above the zero-point as a function of arc length along the MP2/6-311++G** reaction path for the asymmetric CH_2 wag (▲), symmetric CH_2 wag (dashed line), and HF stretch (solid line) for the calculation with negligible excess energy (0.01 kcal/mol).

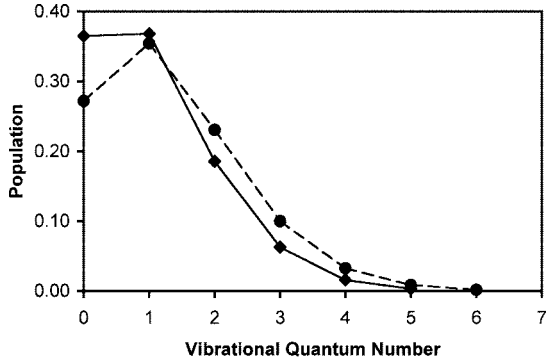

Figure 12. Comparison of HF stretch populations from MP2/6-311++G** quantum-classical calculations at $s = 2.50$ amu$^{1/2}$ bohr, performed with negligible (0.01 kcal/mol, ◆/solid line) and 3.45 kcal/mol (●/dashed line) excess reaction coordinate translational energy. The values in each case are normalized to the sum of all significantly populated HF stretch vibrational levels.

The energy-partitioning results for the calculation performed with a larger amount of TS excess translational energy (3.45 kcal/mol) display roughly the same curve shapes as those in Figures 10 and 11, except with a greater initial value for the kinetic energy. For this case, the vibrational energy of the system increases by approximately 17 kcal/mol in going from TS to products, as compared to about 13 kcal/mol in the negligible excess energy case.

The HF vibrational level distributions at the end of the reaction ($s = 2.50$ amu$^{1/2}$ bohr) for the different initial excess translational energies are displayed in Figure 12. A population inversion is observed for both initial conditions. It can be seen that increasing the reaction coordinate translational energy (from 0.01 to 3.45 kcal/mol) notably increases the magnitude of the inversion. Hence, starting with more energy in translation allows more energy to be siphoned into HF vibration by the curvature.

The MP2/6-311++G** results for the HF stretch vibrational state populations can be compared to those obtained experimentally and theoretically. IRMPD experiments, such as those of Quick and Wittig,[17] are thought to dissociate molecules with minimal excess energy, although it is almost certainly more than the amounts used in our calculations. The chemical activation process $H + C_2H_4F \rightarrow [C_2H_5F]^{\ddagger}$, as performed by Arunan et al.,[19] imparts an excess energy of approximately 42 kcal/mol to the dissociating C_2H_5F. The experimental results can still be compared to our calculations done with lower excess energies to observe the role of the potential energy release in the

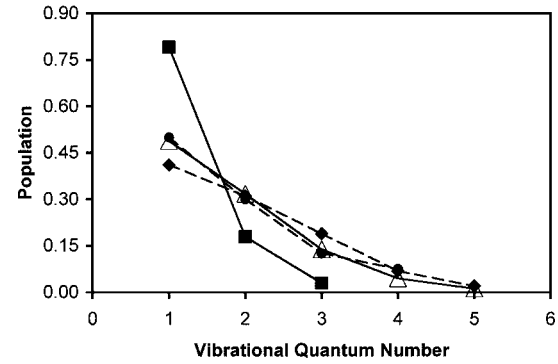

Figure 13. Comparison of HF stretch populations from theoretical (solid line) and experimental (dashed line) studies, for the cases where the theoretical excess translational energy was taken to be 3.45 kcal/mol. Our MP2/6-311++G** quantum-classical results are shown as △, the MP2/6-311++G** direct dynamics results (ref 34) as ■, the IRMPD results (ref 17) as ●, and the chemical activation results (ref 19) as ◆. In all cases, the results are normalized to the sum of the populations of the first five excited vibrational states.

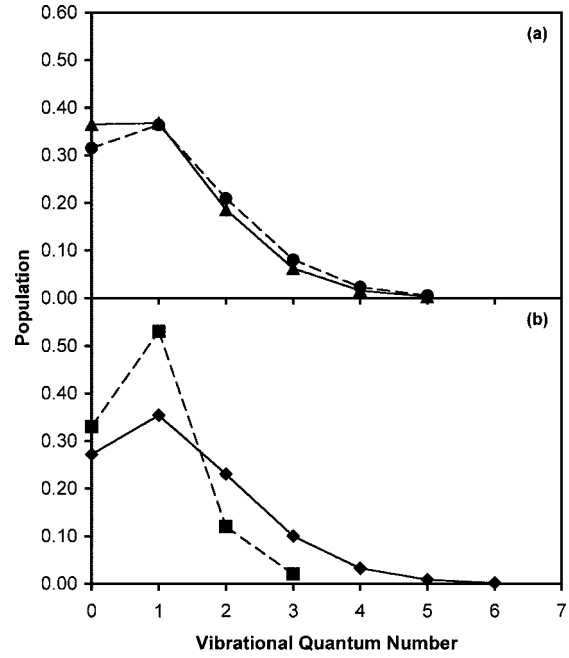

Figure 14. Theoretical dynamics comparisons, including the ground state. (a) Comparison of HF stretch populations from our MP2/6-311++G** quantum-classical calculations (▲/solid line) to our B3LYP/6-311++G(2d,2p) quantum-classical calculations (●/dashed line), for the negligible excess energy case. (b) Comparison of HF stretch populations from our MP2/6-311++G** quantum-classical calculations (◆/solid line) to MP2/6-311++G** direct dynamics calculations (■/dashed line, ref 34), for the case where the excess translational energy is 3.45 kcal/mol. The results in all cases are normalized to the sum of all significantly populated HF stretch vibrational levels.

dynamics. These comparisons are shown in Figures 9 (0.01 kcal/mol) and 13 (3.45 kcal/mol), in which all results are renormalized to the sum of the populations of the first five excited states because the ground-state populations were only estimated in the experiments, as emission was monitored. A comparison to the direct dynamics quasiclassical trajectory simulations performed by Dong et al.[34] with the same level of theory, basis set, and excess translational energy is also shown in Figure 13. A comparison to the direct dynamics study that includes the ground-state populations is displayed in Figure 14b. Figure 14a compares our MP2/6-311++G** results to our B3LYP/6-311++G(2d,2p) results for the negligible excess energy case.

TABLE 3: Energy Partitioning to the Product Degrees of Freedom

	potential energy partitioning				total energy partitioning[a]	
product motion	B3LYP Q/C	MP2 Q/C	MP2 dir. dyn.[b]	expt.[c]	MP2 Q/C	MP2 dir. dyn.[b]
HF vibration	28.2% (12.2)[d]	22.1% (11.3)	18%	24%	26.7% (14.5)	16.9%
C_2H_4 vibration	5.4% (2.3)	4.1% (2.1)	2%		3.9% (2.1)	6.8%
translation and rotation	66.5% (28.7)	73.8% (37.6)	81%		69.3% (37.7)	76.3%

[a] For 3.45 kcal/mol excess reaction coordinate translational energy. [b] Reference 34. [c] References 17 and 19. [d] Values in parentheses are energies in kcal/mol.

The results shown in Figure 9 (negligible excess energy) seem to indicate that most of the HF excitation arises from the potential energy release, as suggested by Quick and Wittig and Arunan et al.,[17,19] and that the excitation is not largely dependent on the excess energy of the system, because our results are similar to those of experimental studies that provided a much greater deal of excess energy to the system. From Figures 9 and 14a, it can also be seen that our MP2/6-311++G** results compare well with our B3LYP/6-311++G(2d,2p) results, due to the similar reaction paths followed. Increasing the initial translational kinetic energy in our calculations to 3.45 kcal/mol yields excellent agreement with the IRMPD experimental results of Quick and Wittig (Figure 13) by allowing greater excitation of higher energy states. In addition, Figure 13 shows that the agreement with the results of chemical activation experiments is also fairly good even at this low level of excess energy. The good agreement with IRMPD experimental results from our calculation with 3.45 kcal/mol excess translational energy is consistent with the argument of Quick and Wittig that the excess energy only slightly perturbs the HF vibrational level populations.[17]

The agreement between our results and the direct dynamics quasiclassical trajectory studies for the HF vibrational level populations is fairly good (see Figures 13 and 14b), although there are a few differences. The agreement is best for states beyond the first excited state, and both studies predict a population inversion. When the quasiclassical trajectory simulations were performed at greater excess energies than modeled with our method, the vibrational population inversion decreased with increasing excess energy,[34] while our inversion magnitude tends to increase with increasing energy (Figure 12). This could be due to the fact that the greater amounts of excess energy were statistically distributed at the TS in the trajectory simulations, whereas our data in Figure 12 originate from having only the zero-point energy in the TS normal modes. We also generally predict slightly greater populations in higher energy states.

Relationships can be found between the TS energy and the energy partitioning in the products using Zamir and Levine's prediction:[36]

$$\langle E_i \rangle = E_i^\circ + a_i E^\ddagger \tag{22}$$

where $\langle E_i \rangle$ is the average value of a type of product energy (i), E_i° is the amount of the potential energy release (E°) given to product energy i, and a_i is the fraction of $E^\ddagger$, the TS excess energy, partitioned to product energy i. The direct dynamics trajectory studies included linear regression of $\langle E_i \rangle$ versus $E^\ddagger$.[33,34] When extrapolated to zero excess energy, the energy released to each type of product motion arising from the potential could be determined. Our studies give the product energies of HF vibration, C_2H_4 vibration, and reaction path translation. However, our translational energy value also contains some rotational energy from the TS vibrational modes that are exponentially forced to zero, whose energy is returned to translation. The remaining potential energy at $s = 2.50$ amu$^{1/2}$ bohr (8.5 kcal/mol for B3LYP and 11.7 kcal/mol for MP2) is assumed to be partitioned solely into translation, because the curvature is negligibly small after this point. The fractions of the potential energy partitioned to each product energy type are given in Table 3. Our reaction path translational energy in the table is termed "translation and rotation" for the above reason.

The data in Table 3 can be compared to both experimental and computational studies. The translational and rotational energy fractions determined in other studies can be summed together for a somewhat reasonable comparison to our "translation and rotation" fraction, because we do not explicitly account for rotational motions. In summarizing multiple experiments on haloalkanes, it is suggested that the potential energy releases as 32% relative translation and HF rotation, 45% C_2H_4 vibration and rotation, and 24% HF vibration.[19] In contrast, the direct dynamics study concluded that the potential energy release goes as 81% relative translation and rotation, 2% C_2H_4 vibration, and 18% HF vibration.[34] From Table 3, our data agree with the findings of the direct dynamics study that more of the potential energy is released to relative translation than to C_2H_4 vibration. The larger experimental value for C_2H_4 vibration has been suggested to be a potential mass effect problem caused by generalizing CH_3CCl_3 dissociation data to the lighter C_2H_5F.[33−35] Hence, the only experimental value listed in Table 3 is for HF vibration, which was the only parameter directly measured for C_2H_5F decomposition. Good agreement is obtained with both experiment and trajectory calculations as to the fraction of the potential released to HF vibration.

It was mentioned earlier that our B3LYP reaction path had lost more potential energy by the end of major curvature than our MP2 path. Because of conservation of energy, a greater loss of potential energy allows more energy to be funneled into vibration by the curvature; this is reflected in the HF vibrational excitation, as HF ended up with more vibrational energy in the dynamics calculation performed on the B3LYP path (28% of the potential) than on the MP2 path (22% of the potential). Another reason for this difference is the greater magnitude of the HF stretch curvature coupling element obtained in the B3LYP calculation (Figure 5). Even though the B3LYP energetics did not agree as well with experiment (Table 2), the energy-partitioning dynamics are similar to the MP2 results; this suggests that less-expensive DFT methods can continue to be used in studies of this sort.

The right side of Table 3 shows a comparison of general trends in product energy partitioning for the 3.45 kcal/mol excess translational energy calculations. We see the same trend as the quasiclassical trajectory results,[34] except that we again predict a larger fraction of energy is partitioned to HF vibration. If a

calculation was performed with nonzero initial excited vibrational state populations, it is expected that we would observe increasing energy partitioning to C_2H_4 vibration with increasing amounts of excess energy beyond 3.45 kcal/mol.

To summarize the comparisons of this section, our mixed quantum-classical approach to modeling C_2H_5F decomposition using the MP2/6-311++G** level of theory gives fairly good agreement with both experiment and direct dynamics trajectory simulations done at the same level of theory and basis set. As in the direct dynamics study,[34] we observe an inversion of the HF vibrational state populations, but our method predicts slightly higher populations of HF excited vibrational states than the corresponding trajectory simulation. The data also agree with direct dynamics studies that a majority of the potential energy release goes into relative product translation, rather than olefin fragment vibration and rotation. However, our model agrees very well with both IRMPD[17] and chemical activation[19] experiments as to the fraction of the potential energy release yielded to HF vibration. Our MP2/6-311++G** results are also similar to our B3LYP/6-311++G(2d,2p) results for HF elimination, reflecting the similar reaction paths followed.

IV. Summary

We present here a mixed quantum-classical treatment based on the reaction path Hamiltonian of Miller, Handy, and Adams[44] that predicts vibrational excitation due to reaction path curvature in the exit channel. We use a time-dependent perturbation approach for which the mode-path curvature coupling is treated as the perturbation. The resultant equations are then used to determine the energy-partitioning dynamics along the MEP. The computational effort of this treatment scales essentially with the effort of computing the force constants, and not directly with the number of atoms. Here, we have calculated the dynamics on the B3LYP/6-311++G(2d,2p) and MP2/6-311++G** reaction paths for HF elimination from fluoroethane. By using a negligible amount of excess energy, we were able to observe the role of the potential energy release in HF vibrational excitation.

We compared our final vibrational state populations of HF with the experimental results of Quick and Wittig (IRMPD)[17] and Arunan et al. (chemical activation)[19] and the computational results of Dong et al. (direct dynamics quasiclassical trajectory simulations).[34] Generally, both MP2 and B3LYP quantum-classical dynamics showed good agreement with IRMPD results. Fair agreement was also observed with chemical activation results, even though the amount of excess energy in those studies is much greater. While one may expect an IRMPD experiment could be modeled with minimal initial excess energy, Quick and Wittig reported that they expected an excess energy of 20−35 kcal/mol with their experimental setup. The agreement between results supports the arguments made that the majority of the HF vibrational excitation arises from the potential energy release.[17,19] Our results followed trends similar to those of classical trajectory calculations utilizing the same level of theory and basis set. Most notably, we agree that roughly 20% of the potential energy releases as HF vibration, and, in contrast to experiment, much more of the potential is released to translation than ethylene vibration.

In conclusion, our calculations give good qualitative agreement with both experiment and quasiclassical trajectory simulations for the reaction studied. This method could prove useful in predicting the trends for population distributions in unimolecular reactions. Additional systems are currently under investigation.

Acknowledgment. This material is based on work supported by the Mechanics Division of the Office of Naval Research. We thank the NDSU Center for High Performance Computing for the use of their computational resources.

References and Notes

(1) Berry, M. J.; Pimentel, G. C. *J. Chem. Phys.* **1968**, *49*, 5190.
(2) Clough, P. N.; Polanyi, J. C.; Taguchi, R. T. *Can. J. Chem.* **1970**, *48*, 2919.
(3) Setser, D. W.; Chang, H. W.; Perona, M. J. *J. Phys. Chem.* **1971**, *75*, 2070.
(4) Chang, H. W.; Craig, N. L.; Setser, D. W. *J. Phys. Chem.* **1972**, *76*, 954.
(5) Kim, K. C.; Setser, D. W.; Holmes, B. E. *J. Phys. Chem.* **1973**, *77*, 725.
(6) Kim, K. C.; Setser, D. W. *J. Phys. Chem.* **1973**, *77*, 2021.
(7) Kim, K. C.; Setser, D. W. *J. Phys. Chem.* **1974**, *78*, 2166.
(8) Sirkin, E. R.; Berry, M. J. *IEEE J. Quantum Electron.* **1974**, *QE-10*, 701.
(9) Holmes, B. E.; Setser, D. W. *J. Phys. Chem.* **1975**, *79*, 1320.
(10) Holmes, B. E.; Setser, D. W. *J. Phys. Chem.* **1978**, *82*, 2450.
(11) Holmes, B. E.; Setser, D. W. *J. Phys. Chem.* **1978**, *82*, 2461.
(12) Tschuikow-Roux, E.; Quiring, W. J.; Simmie, J. M. *J. Phys. Chem.* **1970**, *74*, 2449.
(13) Tschuikow-Roux, E.; Millward, G. E.; Quiring, W. J. *J. Phys. Chem.* **1971**, *75*, 3493.
(14) Richardson, T. H.; Setser, D. W. *J. Phys. Chem.* **1977**, *81*, 2301.
(15) Sudbo, A. S.; Schulz, P. A.; Shen, Y. R.; Lee, Y. T. *J. Chem. Phys.* **1978**, *69*, 2312.
(16) Quick, C. R., Jr.; Wittig, C. *J. Chem. Phys.* **1978**, *69*, 4201.
(17) Quick, C. R., Jr.; Wittig, C. *J. Chem. Phys.* **1980**, *72*, 1694.
(18) Ishikawa, Y.; Arai, S. *Bull. Chem. Soc. Jpn.* **1984**, *57*, 2040.
(19) Arunan, E.; Wategaonkar, S. J.; Setser, D. W. *J. Phys. Chem.* **1991**, *95*, 1539.
(20) Seakins, P. W.; Woodbridge, E. L.; Leone, S. R. *J. Phys. Chem.* **1993**, *97*, 5633.
(21) McDoniel, J. B.; Holmes, B. E. *J. Phys. Chem. A* **1997**, *101*, 1334.
(22) Ferguson, H. A.; Ferguson, J. D.; Holmes, B. E. *J. Phys. Chem. A* **1998**, *102*, 5393.
(23) Rajakumar, B.; Reddy, K. P. J.; Arunan, E. *J. Phys. Chem. A* **2002**, *106*, 8366.
(24) Setser, D. W.; Muravyov, A. A.; Rengarajan, R. *J. Phys. Chem. A* **2004**, *108*, 3745.
(25) Ferguson, J. D.; Johnson, N. L.; Kekenes-Huskey, P. M.; Everett, W. C.; Heard, G. L.; Setser, D. W.; Holmes, B. E. *J. Phys. Chem. A* **2005**, *109*, 4540.
(26) Hiberty, P. C. *J. Am. Chem. Soc.* **1975**, *97*, 5975.
(27) Kato, S.; Morokuma, K. *J. Chem. Phys.* **1980**, *73*, 3900.
(28) Benito, R. M.; Santamaria, J. *J. Phys. Chem.* **1988**, *92*, 5028.
(29) Raff, L. M.; Graham, R. W. *J. Phys. Chem.* **1988**, *92*, 5111.
(30) Toto, J. L.; Pritchard, G. O.; Kirtman, B. *J. Phys. Chem.* **1994**, *98*, 8359.
(31) Martell, J. M.; Beaton, P. T.; Holmes, B. E. *J. Phys. Chem. A* **2002**, *106*, 8471.
(32) Rajakumar, B.; Arunan, E. *Phys. Chem. Chem. Phys.* **2003**, *5*, 3897.
(33) Sun, L.; Hase, W. L. *J. Chem. Phys.* **2004**, *121*, 8831.
(34) Dong, E.; Setser, D. W.; Hase, W. L.; Song, K. *J. Phys. Chem. A* **2006**, *110*, 1484.
(35) Sun, L.; Park, K.; Song, K.; Setser, D. W.; Hase, W. L. *J. Chem. Phys.* **2006**, *124*, 064313.
(36) Zamir, E.; Levine, R. D. *Chem. Phys.* **1980**, *52*, 253.
(37) Berry, M. J. *J. Chem. Phys.* **1974**, *61*, 3114.
(38) Page, M. *Comput. Phys. Commun.* **1994**, *84*, 115.
(39) Takayanagi, T.; Yokoyama, A. *Bull. Chem. Soc. Jpn.* **1995**, *68*, 2245.
(40) Martínez-Núñez, E.; Estévez, C. M.; Flores, J. R.; Vázquez, S. A. *Chem. Phys. Lett.* **2001**, *348*, 81.
(41) González-Vázquez, J.; Fernández-Ramos, A.; Martínez-Núñez, E.; Vázquez, S. A. *J. Phys. Chem. A* **2003**, *107*, 1389.
(42) González-Vázquez, J.; Fernández-Ramos, A.; Martínez-Núñez, E.; Vázquez, S. A. *J. Phys. Chem. A* **2003**, *107*, 1398.
(43) Martínez-Núñez, E.; Vázquez, S. *J. Chem. Phys.* **2004**, *121*, 5179.
(44) Miller, W. H.; Handy, N. C.; Adams, J. E. *J. Chem. Phys.* **1980**, *72*, 99.
(45) Billing, G. D. *Chem. Phys.* **1984**, *89*, 199; **1989**, *135*, 423; **1990**, *146*, 63.
(46) González, J.; Giménez, X.; Bofill, J. M. *J. Phys. Chem. A* **2001**, *105*, 5022.
(47) González, J.; Giménez, X.; Bofill, J. M. *J. Chem. Phys.* **2002**, *116*, 8713.

(48) González, J.; Giménez, X.; Bofill, J. M. *Theor. Chem. Acc.* **2004**, *112*, 75.

(49) Miller, W. H. *J. Phys. Chem.* **1983**, *87*, 3811.

(50) Miller, W. H. In *Stochasticity and Intramolecular Redistribution of Energy*; Lefebvre, R., Mukamel, S., Eds.; Reidel: Boston, 1987; p 263.

(51) Miller, W. H. In *New Theoretical Concepts for Understanding Organic Reactions*; Bertrán, J., Csizmadia, I. G., Eds.; Kluwer: Dordrecht, Netherlands, 1989; p 347.

(52) Makri, N.; Miller, W. H. *J. Chem. Phys.* **1987**, *87*, 5781.

(53) Fang, J.-Y.; Hammes-Schiffer, S. *J. Chem. Phys.* **1998**, *108*, 7085; **1998**, *109*, 7051.

(54) Billing, G. D. *Int. Rev. Phys. Chem.* **1994**, *13*, 309.

(55) Kraka, E. In *Encyclopedia of Computational Chemistry*; Schleyer, P. v. R., Allinger, N. L., Clark, T., Gasteiger, J., Kollman, P. A., Schaefer, H. F., III, Schreiner, P. R., Eds.; Wiley: Chichester, U.K., 1998; Vol. 4, p 2437.

(56) A preliminary version of this method has been applied to the unimolecular decomposition of methylene nitramine via HONO elimination, see: Stopera, C.; Page, M. *Theor. Comput. Chem.* **2003**, *13*, 53.

(57) (a) Aprà, E.; Windus, T. L.; Straatsma, T. P.; Bylaska, E. J.; de Jong, W.; Hirata, S.; Valiev, M.; Hackler, M.; Pollack, L.; Kowalski, K.; Harrison, R.; Dupuis, M.; Smith, D. M. A.; Nieplocha, J.; Tipparaju,V.; Krishnan, M.; Auer, A. A.; Brown, E.; Cisneros, G.; Fann, G.; Fruchtl, H.; Garza, J.; Hirao, K.; Kendall, R.; Nichols, J.; Tsemekhman, K.; Wolinski, K.; Anchell, J.; Bernholdt, D.; Borowski, P.; Clark, T.; Clerc, D.; Dachsel, H.; Deegan, M.; Dyall, K.; Elwood, D.; Glendening, E.; Gutowski, M.; Hess, A.; Jaffe, J.; Johnson, B.; Ju, J.; Kobayashi, R.; Kutteh, R.; Lin, Z.; Littlefield, R.; Long, X.; Meng, B.; Nakajima, T.; Niu, S.; Rosing, M.; Sandrone, G.; Stave, M.; Taylor, H.; Thomas, G.; van Lenthe, J.; Wong, A.; Zhang, Z. *NWChem, A Computational Chemistry Package for Parallel Computers, Version 4.7*; Pacific Northwest National Laboratory: Richland, WA, 2005, a modified version. (b) Kendall, R. A.; Aprà, E.; Bernholdt, D. E.; Bylaska, E. J.; Dupuis, M.; Fann, G. I.; Harrison, R. J.; Ju, J.; Nichols, J. A.; Nieplocha, J.; Straatsma, T. P.; Windus, T. L.; Wong, A. T. *Comput. Phys. Commun.* **2000**, *128*, 260.

(58) Page, M.; Doubleday, C.; McIver, J. W., Jr *J. Chem. Phys.* **1990**, *93*, 5634.

(59) NIST Computational Chemistry Comparison and Benchmark Database. *NIST Standard Reference Database Number 101, Release 14*; Johnson, R. D., III, Ed.; September, 2006; http://srdata.nist.gov/cccbdb.

(60) Lynch, B. J.; Truhlar, D. G. *J. Phys. Chem. A* **2001**, *105*, 2936.

JP806071G